# Evidence for the Critical Role of Nanoscale Surface Roughness on the Retention and Release of Silver Nanoparticles in Porous Media

Yan Liang<sup>1, 2</sup>, Jini Zhou<sup>1</sup>, Yawen Dong<sup>1</sup>, Erwin Klumpp<sup>3</sup>, Jiří Šimůnek <sup>4</sup>, and Scott A. Bradford<sup>5\*</sup>

<sup>1</sup>School of Resources, Environment and Materials, Guangxi University, Nanning, China

<sup>2</sup>Guangxi Key Laboratory for Agro-Environment and Agro-Product Safety, Nanning, China

<sup>3</sup>Agrosphere Institute, IBG-3, Forschungszentrum Jülich GmbH, Jülich, Germany

<sup>4</sup>Department of Environmental Sciences, University of California, Riverside, CA, United

States

<sup>5</sup>US Salinity Laboratory, USDA, ARS, Riverside, CA, United States

<sup>\*</sup> Corresponding Author phone: +1 951 3694857; Fax: +1 951 3424964; email: scott.bradford@ars.usda.gov

Abstract – Although nanoscale surface roughness has been theoretically demonstrated to be a

crucial factor in the interaction of colloids and surfaces, little experimental research has investigated

the influence of roughness on colloid or silver nanoparticle (AgNP) retention and release in porous

media. This study experimentally examined AgNP retention and release using two sands with very

different surface roughness properties over a range of solution pH and/or ionic strength (IS). AgNP

transport was greatly enhanced on the relatively smooth sand in comparison to the rougher sand, at

higher pH, and lower IS and fitted model parameters showed systematic changes with these

physicochemical factors. Complete release of the retained AgNPs was observed from the relatively

smooth sand when the solution IS was decreased from 40 mM NaCl to deionized (DI) water and

then the solution pH was increased from 6.5 to 10. Conversely, less than 40% of the retained

AgNPs was released in similar processes from the rougher sand. These observations were

explained by differences in the surface roughness of the two sands which altered the energy barrier

height and the depth of the primary minimum with solution chemistry. Limited numbers of AgNPs

apparently interacted in reversible, shallow primary minima on the smoother sand, which is

consistent with the predicted influence of a small roughness fraction (e.g., pillar) on interaction

energies. Conversely, larger numbers of AgNPs interacted in deeper primary minima on the

rougher sand, which is consistent with the predicted influence at concave locations. These findings

highlight the importance of surface roughness and indicate that variations in sand surface roughness

can greatly change the sensitivity of nanoparticle transport to physicochemical factors such as IS

and pH due to the alteration of interaction energy and thus can strongly influence nanoparticle

mobility in the environment.

**Keywords**: surface roughness; AgNPs; XDLVO; retention; release.

2

#### 1. Introduction

The transport and retention of colloids (e.g., microorganisms, clays, organic matter, and nanoparticles) in porous media strongly influences their fate in the environment (Bradford et al. 2002, Wang et al. 2016, Fazeli Sangani et al. 2018, Molnar et al. 2019). Colloid filtration theory considers that retention in porous media is dependent on the mass transfer rate from the bulk solution to the collector surface, and the sticking efficiency on the collector (grain) surface (Yao et al. 1971). Several correlation equations have been developed to predict the colloid mass transfer rate to collector surfaces as a function of the water velocity, the size of the colloid and the collector, and the colloid density (Tufenkji and Elimelech 2004, Messina et al. 2015). The sticking efficiency has commonly been related to the solution chemistry (e.g., pH, ionic strength, cation type), flow velocity (Torkzaban et al. 2007, Shen et al. 2010), and the size and surface properties (charge, surface coating) of the collector and colloid (Lin et al. 2011, Flory et al. 2013, Park et al. 2016).

The sticking efficiency of colloids on collector surfaces is normally related to interaction energy calculations which are used to determine the favorability and strength of colloid adhesion. The interaction energy is frequently assumed to depend on the Derjaguin-Landau-Verwey-Overbeek (DLVO) theory (Derjaguin and Landau 1941, Verwey and Overbeek 1948). Interaction energy calculations normally assume that the colloid and collector surfaces are chemically homogeneous and smooth. In contrast, the surface of natural porous media exhibits pronounced roughness, which can be as high as several hundreds of nanometers or micrometers for a sand surface (Shellenberger and Logan 2002, Shen et al. 2011, Konopinski et al. 2012, Jin et al. 2015, Rasmuson et al. 2017, Johnson et al. 2018, Rasmuson et al. 2019, Ron et al. 2019). It has been widely acknowledged that surface roughness is one of the important factors causing deviations between experimental and theoretical results (Rabinovich et al. 2000, Katainen et al. 2006). The roughness properties of a collector and colloid are important for predicting colloid retention (Jin et al. 2015, Ron et al. 2019). Surface roughness can dramatically alter the colloid retention and

release by altering the interaction energy profiles. For example, the repulsive energy barrier and depths of the primary and secondary minima are lowered or eliminated on top of nanoscale convex asperities, and the energy barrier can be eliminated and the depth of the primary minimum can be increased at the bottom of nanoscale convex asperities (Suresh and Walz 1996, Bhattacharjee et al. 1998, Hoek et al. 2003, Hoek and Agarwal 2006, Bradford and Torkzaban 2013, Shen et al. 2019). In addition, surface roughness will modify the flow field adjacent to the solid surface, increase the lever arm for the resisting adhesive torque, and decrease and/or eliminate the lever arm for the applied hydrodynamic torque (Burdick et al. 2005, Bradford et al. 2013). These roughness effects can enhance colloid retention on electrostatically repulsive surfaces and diminish retention on electrostatically attractive surfaces (Bradford et al. 2017). Weaker adhesive interactions on rough surfaces contribute to colloid removal by diffusion and/or hydrodynamics (Bradford and Torkzaban 2015) and can explain colloid release from primary minima under increasingly unfavorable conditions (Shen et al. 2018). Coupled effects of hydrodynamic slip and colloid-surface interactions with asperities can decrease the gap between favorable and unfavorable conditions and influence colloid detachment during ionic strength (IS) and flow perturbations (Rasmuson et al. 2019, Ron et al. 2019). Bradford et al. (2017) demonstrated that roughness conditions that contribute to colloid retention change with the solution chemistry and charge of surfaces. Although theoretical calculations have demonstrated that surface roughness has a large influence on colloid retention and release, relatively little experimental research has examined these issues, especially under different solution chemistry conditions (Shen et al. 2011, Shen et al. 2012, Torkzaban and Bradford 2016, Rasmuson et al. 2019). Furthermore, this experimental research has not been compared with theoretical calculations that account for nanoscale roughness.

Silver nanoparticles (AgNPs) are one of the most widely used nanomaterials (Nowack et al. 2011, Vance et al. 2015). There is concern about the inevitable release of AgNPs into the environment (Yu et al. 2013, McGillicuddy et al. 2017) and the potential adverse effect on human

health and the environment (León-Silva et al. 2016, Rezvani et al. 2019). Various physicochemical factors have been demonstrated to strongly influence the transport of AgNPs, e.g., grain size of the collector, the solution IS and pH, and the presence of stabilizers (Lin et al. 2011, Flory et al. 2013, Liang et al. 2013b, Park et al. 2016, Adrian et al. 2018, Neukum 2018). However, previous transport studies may provide incorrect or incomplete interpretations because they have largely neglected the role of nanoscale surface roughness on AgNP retention and release. In this work, AgNP transport experiments were therefore conducted in mixtures of two sands with the same size range and surface chemical properties, but very different surface roughness conditions. The retention behavior of AgNPs on these sands was studied under various solution IS and pH. Interaction energy calculations that accounted for various sand roughness properties and numerical simulations were performed to deduce the governing mechanisms of retention and release. The findings from this study improve our understanding and description of colloid interactions and transport behavior in the environment.

### 2. Materials and Methods

# 2.1 Solution chemistry

Ultrapure water and KNO<sub>3</sub> were used to make electrolyte solutions with an IS of 5, 10, 20, 40, and 50 mM. The unadjusted pH of these solutions was around 6.5. NaOH and HNO<sub>3</sub> were employed to adjust the pH values in some 5 mM KNO<sub>3</sub> solutions to 4, 8, 8.5, 9.0, and 10.

# 2.2 Quartz sand

Two analytically pure quartz sands were employed in column experiments. One was purchased from Quarzwerke GmbH, Germany (denoted as QW sand) and was prepared by cleaning and sieving of natural raw materials, whereas the other was obtained from Tianjin Guangfu Fine Chemical Research Institute, China (denoted as GF sand) and was produced by comminution of quartzite. To minimize the influence of chemical heterogeneities on the sand surfaces, purification

procedures for sands were performed, including boiling in HNO<sub>3</sub> and H<sub>2</sub>O<sub>2</sub> in a high borosilicate glass reactor with constant stirring, rinsing with deionized water, and drying to minimize the trace amount of metal oxides and organic impurities (Liang et al. 2013b). Characterization of the sands for physicochemical properties including surface morphology (images and roughness parameters), grain size distribution parameters, specific surface area, streaming potential, and chemical composition (Al, Fe, Mg, and Ca) on the surface was described in section S1 of the supporting information (SI).

# 2.3 AgNPs

Raw AgNP suspension (10.16 % w/w) was purchased from AgPURETM, rent a scientist ® GmbH, Germany. This product was OECD reference NM-Series of representative manufactured nanomaterials (NM-300 silver). The manufacturer reported that the AgNPs were stabilized using a mixture of two non-ionic surfactants, 4% w/w each of Polyoxyethylene Glycerol Trioleate and Polyoxyethylene (20) Sorbitan mono-Laurat (Tween 20). The stability, homogeneity, and solubility of this material were characterized and described in detail in previous research (Kaegi et al. 2011, Klein et al. 2011, Liang et al. 2013b). In general, the AgNPs were spherical and the size measured by the transmission electron microscope (TEM) was 15-20 nm (Liang et al. 2013b). AgNP suspension for each experiment was freshly prepared by diluting the raw concentrated suspension into KNO3 solutions and then sonicated for 15 min in a sonication bath. The initial AgNP suspension concentration was determined to be approximately 10 mg L<sup>-1</sup> using an inductively coupled plasma-mass spectrometry (ICP-MS) after dissolving with 30 % HNO3. The zeta potentials and the hydrodynamic diameters of AgNPs in selected solution chemistries were measured with a ZetaSizer Nano ZS90 (Malvern Instruments, Worcestershire, U.K.) and then used in interaction energy calculations.

Concentrations of AgNPs in transport studies were determined using a UV-Vis spectrophotometer (Thermo Scientific, TM Evolution 300, U.S.) with a fixed scan at a wavelength of 413 nm ( $R^2$  of calibration curves  $\geq 0.9995$  and the detection limit was 0.05 mg/L). The AgNP suspension was determined to be stable by comparison of UV-vis absorbance readings of input AgNP suspensions for the considered solution chemistries (pH from 4 to 10 and IS from 5 to 50 mM KNO<sub>3</sub>) over the duration of experiments. The dissolution of AgNPs was also found to be negligible (less than 1% of the total mass) for similar conditions (Kaegi et al. 2011, Klein et al. 2011, Liang et al. 2013b).

# 2.4 Transport experiments

Water saturated column experiments were performed following the protocols outlined in Liang et al. (2013b). In brief, quartz sand was wet-packed in a stainless-steel column with a 3 cm inner diameter and 12 cm length. A peristaltic pump was used to inject solution and AgNP suspension into the columns in an upflow mode. The input concentration of AgNPs was fixed at 10 mg L<sup>-1</sup> and the Darcy velocity was kept constant at around 0.7 cm min<sup>-1</sup> in all column experiments. Transport experiments were conducted in the following steps: (1) the packed column was conditioned with around 50 pore volumes (PVs) of KNO<sub>3</sub> background solution; (2) 100 mL tracer (KNO<sub>3</sub> solution at 2 to 5-fold concentration of the background solution) was introduced into the column followed by irrigation of at least 5 PVs background solution; (3) 100 mL AgNP suspension was then injected into the column and rinsed by around 3 PVs of the same KNO<sub>3</sub> solution until the normalized concentration was less than 1%. Breakthrough curves (BTCs) of tracer were determined from conductivity measurement on collected effluent samples, whereas BTCs of AgNPs were obtained by determining the concentrations of effluent samples using a UV-Vis spectrophotometer.

**Mixtures of QW and GF sands** - Two types of sand with different surface structures and properties at mass ratios of QW:GF=0:1, 1:2, 1:1, 2:1, and 1:0 were homogeneously mixed before

they were packed into the columns for transport experiments. The IS was 5 mM KNO<sub>3</sub> and the other experimental procedures were the same as described above.

**Transport of AgNPs under different IS** - Column experiments were carried out to investigate the retention of AgNPs on a relatively smooth GF sand surface under different IS (5, 10, 20, 40, and 50 mM KNO<sub>3</sub>) conditions.

**Different pH values of the column system** - pH values of 4.0, 6.5 (unadjusted), 8.0, 8.5, 9.0, and 10 were selected for each column experiment using rough QW sand at IS of 5 mM, while pH values of 6.5 (unadjusted) and 8.0 were selected for experiments with GF sand at IS=50 mM. The pH in KNO<sub>3</sub>, tracer, and AgNP suspension were all adjusted to a selected value in a given column experiment.

# 2.5 Release experiments

AgNPs were initially retained in the presence of 5 mM KNO<sub>3</sub> on rough QW sand and 40 mM KNO<sub>3</sub> on relatively smooth GF sand in a similar manner to section 2.4 and then subject to a 20-hour flow interruption (phase I). The release of AgNPs was then initiated by flushing the column with several PVs of ultrapure water: (i) with an unadjusted pH (pH 6.5) (phase II); (ii) at pH=10 (phase III); and (iii) at pH=10 after a 20 h flow interruption (phase IV). Finally, the sand was excavated from the column and placed into a container containing excess amounts of ultrapure water at pH 10 (phase V). The container was slowly shaken for several minutes to investigate the release of the remaining retained AgNPs by determination of the AgNP concentration, the volume of water, and the mass of dry sand.

# 2.6 Theory and Model

Interaction energy calculations that considered various surface roughness properties and numerical simulations were performed to better understand mechanisms contributing to AgNP retention and release under the tested solution chemistries. The interaction energy calculations

based on conventional DLVO theory (smooth surface) was applied with and without consideration of steric interactions. The approach of Bradford et al. (2017) was employed to determine the interaction energy ( $\Phi_r$ , MLT<sup>-1</sup>) between AgNP and sand with nanoscale roughness as a linear combination of interaction energies for various nanoscale roughness components. Section S2 of the SI provides details pertaining to these calculations for AgNP-sand interactions. The dimensionless depths of the primary ( $\Phi_{1min}$ ) and secondary ( $\Phi_{2min}$ ) minima, the energy barrier height ( $\Phi_{max}$ ) and the energy barrier to detachment from the primary minimum ( $\Delta \Phi_d = \Phi_{max} - \Phi_{1min}$ ) were obtained by analyzing the interaction energy profiles.

Section S3 in the SI describes the modeling approach in detail. The retention rate coefficient  $(k_1)$  and the normalized maximum solid phase concentration of deposited AgNPs  $(S_{max}/C_o)$ , where  $C_o$  is the AgNP input concentration) for blocking were optimized. The fitted values of  $S_{max}$  were then used to calculate the fraction of the grain surface area that contributes to AgNP retention  $(S_f)$ .

# 3. Results and Discussion

# 3.1 Characterization of AgNPs and quartz sands

Table S1 lists measured zeta potentials of AgNPs and quartz sands, and hydrodynamic diameters ( $d_p$ ) of AgNPs over the range of solution chemistries that were used in column experiments. The zeta potential of AgNPs gradually increased from -22.6  $\pm$  1.6 to -7.4  $\pm$  1.0 mV when the IS increased from 5 to 50 mM KNO<sub>3</sub> at pH=6.5 and became more negative as the pH increased from 4.0 to 10.0 at 5 mM KNO<sub>3</sub>. The AgNP  $d_p$  values slightly increased as the IS increased from 5 to 50 mM KNO<sub>3</sub> at pH=6.5 and decreased as the pH increased from 4.0 to 10.0 at 5 mM KNO<sub>3</sub>. These relatively minor changes in  $d_p$  over a large range in pH and IS reflect the stability of the AgNP suspensions in the presence of adsorbed surfactants (Adrian et al. 2018), which is normally attributed to steric interactions (Hotze et al. 2010). Note that the size determined by the Zeta-sizer is normally larger than by TEM because measurement by the Zeta-sizer is biased

toward a larger size fraction and takes a value of hydrodynamic diameter that can also be influenced by the thickness of the surfactant coating (Diegoli et al. 2008, Klein et al. 2011). The zeta potential of the QW sand decreased from  $-29.0 \pm 0.8$  to  $-57.3 \pm 3.8$  mV when the solution pH increased from 4.0 to 10.0 under 5 mM KNO<sub>3</sub> due to deprotonations of the surface. The zeta potentials of GF sand became less negative when the IS was increased from 5 to 50 mM KNO<sub>3</sub> under pH 6.5 due to compression of the double layer thickness and charge screening.

The mean grain sizes ( $d_{50}$ ) of mixtures with different proportions of rough and relatively smooth sand (mass ratios of 0:1, 1:2, 1:1, 2:1, and 1:0) ranged between 503 and 519 µm, indicating that the two sands were almost at the same size. Microscope images (Figs. S1 and 1) show the significant difference of the surface topography of the two sands. Table S2 presents surface morphological parameters, chemical analysis, and BET surface areas for both purified sands. The average roughness was 418  $\pm$  150 and 78  $\pm$  41 nm for the relatively rough QW and smoother GF sand, respectively, while the surface chemistry and surface area of both sands were generally comparable. Surface roughness is therefore the main difference between the surface properties of these two sands.

# 3.2 Interaction energy calculations

Measured values of  $d_P$  and zeta potential were used to calculate the conventional interaction energy profiles for different IS with (Fig. S2a) and without steric interactions (Fig. S2b). The magnitude of  $\Phi_{2min}$  (<0.33) was always much less than the average kinetic energy fluctuations for diffusing colloids (e.g, 1.5) (Bradford and Torkzaban 2015) and was therefore not considered to contribute to AgNP retention. Parameter values of  $\Phi_{1min}$ ,  $\Phi_{max}$ , and  $\Delta\Phi_d = \Phi_{max} - \Phi_{1min}$  for the AgNP-sand interactions without consideration of steric interaction are given in Table S1. Table S1 shows a general trend of decreasing  $\Phi_{max}$  with decreasing pH and increasing IS because of less negative values of the zeta potentials and compression of the double layer thickness at higher IS. However,

AgNPs can only diffuse over  $\Phi_{max}$  into  $\Phi_{Imin}$  when  $\Phi_{max}$ <6 to 10 (Bradford and Torkzaban 2015). Primary minimum interactions are therefore predicted in GF sand when IS $\geq$ 40 mM and in QW sand when pH=4. No retention is predicted for other solution chemistry conditions. Additionally, if steric interactions from the adsorbed surfactant layer on the AgNPs are included in the interaction energy calculations then a very large energy barrier occurs (Fig. S2b) and no AgNP retention is predicted for all considered solution chemistry conditions. These findings reveal the deviations between experimental results and theoretical calculations based on the conventional interaction energy calculations even if the steric interactions are included.

# 3.3 AgNP retention in the sand with a rough surface

Column experiments were carried out to investigate the influence of sand roughness on AgNP transport and retention by creating quartz sand with different mass ratios of relatively rough QW and smoother GF sands. Fig. 2 shows observed and simulated AgNP BTCs for mixtures of QW and GF sand with mass ratios of 0:1, 1:2, 1:1, 2:1, and 1:0 when the IS=5 mM KNO<sub>3</sub> and pH=6.5 (unbuffered). BTCs were plotted as normalized effluent concentrations ( $C/C_0$ ) versus pore volumes. Table 1 summarizes the experimental conditions, the mass recoveries from BTCs, and the fitted model parameters.

Fig. 2 clearly demonstrates that AgNP retention is significantly different for various mass ratios of these two sands. The mass recovery of AgNPs in the effluent ( $M_{eff}$ ) and the fitted parameters of  $k_1$  and  $S_{max}/C_o$  present an approximately linear correlation with the mass percentage of the relatively rough QW sand to the total amount of quartz sand ( $M_{QW}$ ) (Fig. S3 A1, B1, and C1). Larger  $M_{QW}$  resulted in stronger AgNP retention and larger values of  $k_1$  and  $S_{max}/C_o$  (Table 1). Fig. 2 also shows systematic blocking trends (the gradual ascent trend of the BTCs due to a decrease in AgNP retention over time as retention sites are blocked or filled) which exhibit a delay in AgNP breakthrough and then increasing concentrations of AgNPs in the effluent. These blocking effects

can be explained by the rate of filling of a limited number of retention sites. In particular, blocking/filling of retention sites is expected to occur more rapidly for larger  $k_1$  and smaller  $S_{max}$  (Leij et al. 2015). The value of  $S_f$  (Eq. [S11]) shown in Table 1 was less than 5.3% and 0.8% for geometric and BET surface area estimates, respectively. Consequently, only a very small fraction of the QW sand surface area contributed to AgNP retention. SEM images taken from the samples for both QW and GF sand after completion of transport experiments show large AgNP-free areas (Fig. S4) and this information is consistent with the calculated values of  $S_f$ .

AgNP retention in Fig. 2 is not consistent with interaction energy calculations for smooth and chemical homogeneous surfaces (Fig. S2 and Table S1). In particular, no AgNP retention on the relatively rough QW and GF sands is predicted when the pH=6.5 and the IS=5 mM KNO<sub>3</sub> because  $\Phi_{max}>10$ . Furthermore, differences in AgNP retention on QW and GF sands are not predicted because values of  $\Phi_{max}$  were nearly identical (39.4 and 40.1 for QW and GF sand, respectively). Potential explanations for these discrepancies include nanoscale charge heterogeneity and roughness which can locally reduce and/or eliminate the energy barrier (Suresh and Walz 1996, Bhattacharjee et al. 1998, Hoek et al. 2003, Hoek and Agarwal 2006, Bradford and Torkzaban 2013, Bradford et al. 2017, Bradford et al. 2018). Nanoscale chemical heterogeneity that is larger than a critical size can create regions on a net unfavorable surface that are favorable for interaction between the colloid and the solid surface due to a local reduction in the energy barrier and an increase in the depth of the primary minimum. However, differences in nanoscale chemical heterogeneity are not expected to be the primary cause for the observed AgNP retention behavior on QW and GF sands because: (i) both sands were chemically treated to minimize chemical heterogeneity; (ii) concentrations of major cations in the acid digest of the sands were similar (Table S2); (iii) the predicted energy barrier was nearly identical when using measurements of sand streaming potential (Table S1); and (iv) previous studies have demonstrated that interaction energy profile properties are more sensitive to nanoscale roughness than charge heterogeneity (Bradford et

al. 2017).

Significant differences in the roughness properties of QW and GF sands (Fig. 1, Fig. S1, and Table S2) provide a plausible alternative explanation for differences in AgNP retention in Fig. 2. The energy barrier to the primary minimum at IS=5 mM and pH=6.5 was high enough to inhibit most AgNP retention on the relatively smooth GF sand (Table S1). Conversely, the roughness properties of the QW sand greatly enhanced AgNP retention. Interaction energy calculations have demonstrated that the tops of nanoscale roughness pillars can locally reduce and/or eliminate the energy barrier and the depth of the primary minimum (Shen et al. 2012, Bradford et al. 2017). These roughness effects on interaction energies are magnified for locations with smaller roughness fractions (e.g., pillar diameters) and when roughness occurs on both the colloid and sand surface (Bradford et al. 2017). Diffusive or hydrodynamic removal of colloids from a primary minimum may occur in some cases depending on the local roughness properties (Torkzaban and Bradford 2016, Bradford et al. 2017). Concave locations between protruding roughness asperities also influence the interaction energy profiles (Shen et al. 2012, Li et al. 2017). The energy barrier can be reduced or eliminated at the vertices of these locations because repulsive forces on AgNPs act in opposite directions and cancel out (Li et al. 2017). Colloids that are retained in concave locations are less susceptible to removal by hydrodynamic forces and/or IS reduction than on pillar tops (Li et al. 2017). These observations indicate that the greater  $k_1$ , larger  $S_{\text{max}}/C_0$ , and stronger retardation in the QW sand (Fig. S3) were mainly produced by sand surface roughness properties.

# 3.4 Sensitivity of AgNP retention to pH in rough QW sand

Transport experiments were carried out to better understand the pH dependence of AgNP retention on relatively rough QW sand. Fig. 3 presents observed and simulated BTCs for AgNPs in the relatively rough QW sand when the solution IS = 5 mM KNO<sub>3</sub> and the pH=4.0, 6.5, 8.0, 8.5, 9.0, and 10.0. Results show that an increase in pH resulted in gradual enhancement of AgNP transport.

Fitted values of  $k_1$  and  $S_{\text{max}}/C_o$  when the solution pH=4.0 were nearly 30-fold higher than those obtained when the pH=10.0 (Table 1). Moreover, the fitted  $k_1$  and  $S_{\text{max}}/C_o$  were inversely proportional to the pH values (Fig. S3 B2 and C2). Additionally, the retardation of the AgNP breakthrough was gradually diminished when the solution pH was increased.

AgNP attachment is inhibited or eliminated when  $\Phi_{max}$  is greater than around 5.7 (Bradford and Torkzaban 2015). The value of  $\Phi_{max}$  tends to increase with pH because of more negative zeta potentials and greater electrostatic repulsion (Table S1). This increase in  $\Phi_{max}$  with pH will therefore decrease the roughness effects that contribute to AgNP retention. Table S3 gives an example of the influence of roughness on  $\Phi_{max}$  when pH=4 and 10 and the IS=5 mM. Table 1 also indicates that the fraction of the geometric surface area that contributed to AgNP retention ( $S_f$ ) dramatically decreased from 8.39% to 0.45% as the pH was increased from 4 to 10, respectively. BET estimates of  $S_f$  were even smaller.

# 3.5 AgNP retention in the sand with a relatively smooth surface

Fig. 4 shows observed and simulated AgNP BTCs in the relatively smooth GF sand when the solution IS equaled 5, 10, 20, 40, 50 mM KNO<sub>3</sub> at pH 6.5. Experimental results indicate that the AgNP retention and retardation of the BTCs were significantly increased with the IS. No breakthrough was observed when the IS was 50 mM KNO<sub>3</sub>. A number of column studies have previously observed the trend of increasing AgNP retention (Lin et al. 2011, Liang et al. 2013a, Liang et al. 2013b, Braun et al. 2015) and retardation with IS (Liang et al. 2013a, Adrian et al. 2018). Generally, the optimized simulations provided a good description of the BTCs when AgNPs broke through ( $R^2$ >0.96). Fitted values of  $k_I$  and  $S_{max}/C_o$  systematically increased with IS, whereas calculated  $M_{eff}$  decreased with IS (Table 1). Similar blocking behavior was observed and discussed in section 3.3.

Trends for AgNP BTCs, and fitted and calculated parameters with IS can be partially explained by the decrease in energy barrier with IS when the double layer was compressed (Fig. S2a). However, these interaction energy calculations predict that the entire surface area of the GF sand will equally contribute to AgNP retention and all particles will be retained when the IS=40 and 50 mM. In contrast, Fig. 4 and Table 1 show a systematic difference in the AgNP transport behavior and fitted and calculated parameters with increasing IS. In particular,  $k_1$  and  $S_{max}/C_0$  increase with IS. In addition, calculated values of  $S_f$  in Table 1 indicate that only a small fraction of the GF sand surface area contributed to AgNP retention, even for the favorable condition when the IS=50 mM ( $S_f$  is less than 8.06% and 2.95% for geometric and BET estimates of surface area, respectively).

Significant amounts of nanoscale surface roughness occur even on the relatively smooth GF sand (Table S2). Particularly, the gradual variation of AgNP retention with increasing IS (Fig. 4) further demonstrates the important role of surface roughness, which results in differences in the energy barrier high and the depth of the primary minimum depending on IS. Otherwise, the AgNP retention would vary sharply with increasing IS due to the transition from unfavorable (no retention) to favorable (complete retention) interactions. Research has also demonstrated that the nanoscale roughness fraction has a larger influence on the shape of the interaction energy profile than the roughness height and that a small roughness fraction and height can produce shallow primary minimum on pillar tops that are susceptible to diffusive or hydrodynamic release (Bradford et al. 2017). This can produce portions of the surface area that are unfavorable for AgNP, even when favorable conditions are predicted on smooth surfaces (Zhang et al. 2016, Bradford et al. 2017). Furthermore, the roughness parameters that contribute to irreversible colloid retention have been observed to change and increase with the solution IS (Bradford et al. 2017). Consequently, roughness may also help to explain the trends of AgNP retention with IS (e.g., increasing  $k_1$  and  $S_{max}/C_0$  with IS), even on the relatively smooth GF sand (Bradford et al. 2017).

Fig. S5 presents observed and simulated AgNP BTCs in the relatively smooth GF sand when the solution IS=50 mM KNO<sub>3</sub> and the pH=6.5 and 8.0. The AgNP transport was greatly enhanced when the solution pH was increased from 6.5 (no breakthrough) to 8.0 (78.1% recovered in the effluent). Note that this enhancement in AgNP transport with increasing pH on the relatively smooth GF sand at IS=50 mM (Fig. S5) was much greater than for the rough QW sand at IS=5 mM (Fig. 3). This implies that changes in the interaction energy profile when the pH changed from 6.5 to 8.0 had a larger influence on AgNP retention with the relatively smooth GF sand at IS=50 mM than on the rougher QW sand at IS=5 mM. The probability of AgNPs to diffuse into the primary minimum rapidly increases from 0 to 1 as the energy barrier decreases from around 5.7 to 0 (Bradford and Torkzaban 2015). Consequently, this increased sensitivity to pH likely reflects differences in the energy barrier heights. In particular, AgNP attachment occurs more readily for the lower energy barrier on the GF sand at IS=50 mM than for the higher energy barrier on the QW sand at IS=5 mM (Table S1).

# 3.6 Release of retained AgNPs from quartz sands with different roughness

Additional experiments were conducted to study the release behavior of AgNPs from QW and GF sands. To achieve similar amounts of AgNP retention, the initial deposition occurred at an IS=5 mM KNO<sub>3</sub> and pH=6.5 in the relatively rough QW sand, and for the relatively smooth GF sand an IS=40 mM KNO<sub>3</sub> and pH=6.5 was employed. Fig. 5 presents the release behavior of retained AgNPs under various solution and flow interruption conditions that are summarized in the figure caption. Release phase I consisted of a 20 h flow interruption followed by continued elution with the same particle-free electrolyte solution as during the deposition phase. There was only a negligible amount (0.1%) of AgNPs detected in the effluent for both sands (Table 1). This implies that the retained AgNPs were interacting on the collector surface in a primary minimum that was

strong enough to overcome the strength of diffusion; e.g., the energy barrier to detachment was larger than 5.7.

The eluting solution IS was reduced from 5 and 40 mM KNO<sub>3</sub> for the QW and GF sands, respectively, to that of ultrapure water at pH=6.5 during release phase II (Fig. 5). Only a small fraction of the retained AgNPs was released from the relatively rough QW sand (2.1%), whereas a much larger fraction was released from the relatively smooth GF sand (18.2%). Furthermore, the AgNP release pulse occurred very rapidly from the smoother GF sand and then exhibited lower amounts of release. Note that release with a reduction in IS cannot be explained by the elimination of the secondary minimum because it was not deep enough for colloid immobilization in 5 or 40 mM KNO<sub>3</sub> solution. Furthermore, colloid release with IS reduction from a deep primary minimum from charge heterogeneity on a smooth grain surface is not possible due to an increase in the energy barrier (Shen et al. 2018). Conversely, colloid release with IS reduction may occur from shallow primary minima that happen on tops of nanoscale roughness asperities like pillars (Shen et al. 2018) or fractal surfaces (Shen et al. 2018, Wang et al. 2019), but not from concave locations between roughness asperities because attachment (in primary minima) is irreversible to IS reduction in these valley areas (Li et al. 2017, Wang et al. 2019). The difference in the AgNP release with IS reduction apparently reflects retention on asperities with a shallower primary minimum on the smoother GF sand than the rougher QW sand, e.g., GF sand may contain a smaller roughness fraction or more nanoscale asperities (Wang et al. 2019) than the rougher QW sand.

The pH was increased from 6.5 to 10 while maintaining very low IS conditions (ultrapure water) during phase III of the release experiment (Fig. 5). An additional 14.7% and 70.6% of the retained AgNPs were released from the rougher QW and smoother GF sands, respectively (Table 1). Similar to phase II, AgNP release from the smoother GF sand was again very rapid, and then exhibited lower amounts of release. Conversely, the release of AgNPs from the rougher QW sand was slower than the smoother GF sand, and it gradually reached a peak concentration value at a

later time due to slow diffusive release from deeper primary minima. These trends are generally consistent with those observed during phase II, which were attributed to shallower primary minima on the smoother GF sand due to a smaller roughness fraction. The additional AgNP release when the pH was increased from about 6.5 during phase II to 10 during phase III can be explained by a further decrease and/or elimination of the energy barrier to detachment for certain roughness conditions (Torkzaban and Bradford 2016) when the zeta potential magnitudes were increased (Table S1). Phase IV of the release experiment (Fig. 5) employed a 20 h flow interruption and was followed by continued elution of ultrapure water at pH=10. About 12.8% and 5.0% of the retained AgNPs were released from the rougher QW and smoother GF sands, respectively. Similar release kinetics were observed during phases I through IV. However, a higher release pulse was obtained for the rougher GW than the smoother sand. This occurs because all injected AgNPs were recovered after phase IV from the smoother GF sand (Table 1), while the 20 h flow interruption (after eluting with water at pH 10) allowed for increased time for diffusive release from the shallow primary minima or from low flow regions such as concave locations on the rougher QW sand.

Only 5.2% of retained AgNPs was recovered when the rougher QW sand was excavated from the column and placed in a container with ultrapure water at pH 10 and gently shaken for a few minutes (phase V). Furthermore, less than 40% of the retained AgNPs were collected during release phases I-V for the rougher QW sand. The low total recovery of the AgNPs from the QW sand indicates that remaining AgNPs were retained in a deep primary minimum that was stronger than forces from random kinetic energy fluctuations and/or hydrodynamic shear (Torkzaban and Bradford 2016). Such conditions may occur in surfaces with larger roughness fractions or nanoscale charge heterogeneity on smooth surfaces (Bradford et al. 2018), and/or at concave locations (Shen et al. 2018).

#### 4. Conclusions

Natural porous media commonly exhibit pronounced surface roughness. Experimental results, fitted model parameters, and interaction energy calculations demonstrated that nanoscale roughness on the collector surface controlled AgNP retention and release and that these effects were dependent on the solution chemistry. In particular, limited amounts of AgNPs retention occurred in shallow primary minima (e.g., the tops of small roughness asperities) on the relatively smooth sand that was rapidly released when the IS was reduced and the pH increased. Conversely, much more AgNP retention occurred in deeper primary minima (e.g., concave locations between roughness asperities) on the rougher sand that was mainly irreversible to changes in solution chemistry. Collected data from this study provide valuable information and insight on the importance of roughness on the transport and release of AgNPs, the conditions that enhance or reduce the influence of surface roughness, and the correlation of AgNP deposition parameters with surface roughness. This information also indicates that surface roughness properties of porous media can be optimized to enhance or diminish the retention of colloids and nanoparticles for specific engineering or environmental applications.

# Appendix A. Supplementary data

Supplementary data associated with this article is available free of charge via the Internet.

Acknowledgments –This research was funded by the National Natural Science Foundation of China (Grant NO. 21507015; 51561135012), Guangxi Natural Science Foundation, China (Grant NO. 2015GXNSFCA139015; 2017GXNSFBA198076), and Cultivation Base of Guangxi Key Laboratory for Agro-Environment and Agro-Product Safety (17-259-82). The authors would like to acknowledge the assistance of Dr. Huijun Yao for SEM measurement.

#### References

- Adrian, Y.F., Schneidewind, U., Bradford, S.A., Simunek, J., Fernandez-Steeger, T.M. and Azzam, R., 2018. Transport and retention of surfactant- and polymer-stabilized engineered silver nanoparticles in silicate-dominated aquifer material. Environ. Pollut. 236, 195-207.
- Bhattacharjee, S., Ko, C.-H. and Elimelech, M., 1998. DLVO interaction between rough surfaces. Langmuir 14(12), 3365-3375.
- Bradford, S.A., Kim, H., Shen, C., Sasidharan, S. and Shang, J., 2017. Contributions of nanoscale roughness to anomalous colloid retention and stability behavior. Langmuir 33(38), 10094-10105.
- Bradford, S.A., Sasidharan, S., Kim, H. and Hwang, G., 2018. Comparison of types and amounts of nanoscale heterogeneity on bacteria retention. Front. Environ. Sci. 6(56).
- Bradford, S.A. and Torkzaban, S., 2013. Colloid interaction energies for physically and chemically heterogeneous porous media. Langmuir 29(11), 3668-3676.
- Bradford, S.A. and Torkzaban, S., 2015. Determining parameters and mechanisms of colloid retention and release in porous media. Langmuir 31(44), 12096-12105.
- Bradford, S.A., Torkzaban, S. and Shapiro, A., 2013. A theoretical analysis of colloid attachment and straining in chemically heterogeneous porous media. Langmuir 29(23), 6944-6952.
- Bradford, S.A., Yates, S.R., Bettahar, M. and Simunek, J., 2002. Physical factors affecting the transport and fate of colloids in saturated porous media. Water Resour. Res. 38(12), 63-61-63-12.
- Braun, A., Klumpp, E., Azzam, R. and Neukum, C., 2015. Transport and deposition of stabilized engineered silver nanoparticles in water saturated loamy sand and silty loam. Sci. Total Environ. 535, 102-112.
- Burdick, G.M., Berman, N.S. and Beaudoin, S.P., 2005. Hydrodynamic particle removal from surfaces. Thin Solid Films 488(1), 116-123.

- Derjaguin, B. and Landau, L., 1941. Theory of the stability of strongly charged lyophobic sols and of the adhesion of strongly charged particles in solutions of electrolytes. Acta Physicochimica U.R.S.S. 14, 633-662.
- Diegoli, S., Manciulea, A.L., Begum, S., Jones, I.P., Lead, J.R. and Preece, J.A., 2008. Interaction between manufactured gold nanoparticles and naturally occurring organic macromolecules. Sci. Total Environ. 402(1), 51-61.
- Fazeli Sangani, M., Owens, G. and Fotovat, A., 2018. Transport of engineered nanoparticles in soils and aquifers. Environ. Rev. 27(1), 43-70.
- Flory, J., Kanel, S.R., Racz, L.A., Impellitteri, C.A., Silva, R.G. and Goltz, M.N., 2013. Influence of pH on the transport of silver nanoparticles in saturated porous media: laboratory experiments and modeling. J. Nanopart. Res. 15(15), 1-11.
- Hoek, E.M.V. and Agarwal, G.K., 2006. Extended DLVO interactions between spherical particles and rough surfaces. J. Colloid Interface Sci. 298(1), 50-58.
- Hoek, E.M.V., Bhattacharjee, S. and Elimelech, M., 2003. Effect of membrane surface roughness on colloid–membrane DLVO interactions. Langmuir 19(11), 4836-4847.
- Hotze, E.M., Phenrat, T. and Lowry, G.V., 2010. Nanoparticle aggregation: challenges to understanding transport and reactivity in the environment. J. Environ. Qual. 39, 1909-1924.
- Jin, C., Normani, S.D. and Emelko, M.B., 2015. Surface roughness impacts on granular media filtration at favorable deposition conditions: Experiments and modeling. Environ. Sci. Technol. 49(13), 7879-7888.
- Johnson, W.P., Rasmuson, A., Pazmiño, E. and Hilpert, M., 2018. Why variant colloid transport behaviors emerge among identical individuals in porous media when colloid–surface repulsion exists. Environ. Sci. Technol. 52(13), 7230-7239.

- Kaegi, R., Voegelin, A., Sinnet, B., Zuleeg, S., Hagendorfer, H., Burkhardt, M. and Siegrist, H., 2011. Behavior of metallic silver nanoparticles in a pilot wastewater treatment plant. Environ. Sci. Technol. 45(9), 3902-3908.
- Katainen, J., Paajanen, M., Ahtola, E., Pore, V. and Lahtinen, J., 2006. Adhesion as an interplay between particle size and surface roughness. J. Colloid Interface Sci. 304(2), 524-529.
- Klein, C.L., Comero, S., Locoro, G., Gawlik, B.M., Stahlmecke, B., Romazanov, J. and Kuhlbusch, T.A.J., 2011. NM-series of representative manufactured nanomaterials nm-300 silver characterisation, stability, homogeneity. EUR 24693 EN– Joint Research Centre Institute for Health and Consumer Protection.
- Konopinski, D.I., Hudziak, S., Morgan, R.M., Bull, P.A. and Kenyon, A.J., 2012. Investigation of quartz grain surface textures by atomic force microscopy for forensic analysis. Forensic Sci. Int. 223(1), 245-255.
- León-Silva, S., Fernández-Luqueño, F. and López-Valdez, F., 2016. Silver nanoparticles (AgNP) in the environment: a review of potential risks on human and environmental health. Water Air Soil Pollut. 227(9), 306.
- Leij, F.J., Bradford, S.A., Wang, Y. and Sciortino, A., 2015. Langmuirian blocking of irreversible colloid retention: analytical solution, moments, and setback distance. J. Environ. Qual. 44, 1473-1482.
- Li, T., Jin, Y., Huang, Y., Li, B. and Shen, C., 2017. Observed dependence of colloid detachment on the concentration of initially attached colloids and collector surface heterogeneity in porous media. Environ. Sci. Technol. 51(5), 2811-2820.
- Liang, Y., Bradford, S.A., Simunek, J., Heggen, M., Vereecken, H. and Klumpp, E., 2013a.

  Retention and remobilization of stabilized silver nanoparticles in an undisturbed loamy sand soil.

  Environ. Sci. Technol. 47(21), 12229-12237.

- Liang, Y., Bradford, S.A., Simunek, J., Vereecken, H. and Klumpp, E., 2013b. Sensitivity of the transport and retention of stabilized silver nanoparticles to physicochemical factors. Water Res. 47(7), 2572-2582.
- Lin, S., Cheng, Y., Bobcombe, Y., L. Jones, K., Liu, J. and Wiesner, M.R., 2011. Deposition of silver nanoparticles in geochemically heterogeneous porous media: Predicting affinity from surface composition analysis. Environ. Sci. Technol. 45(12), 5209-5215.
- McGillicuddy, E., Murray, I., Kavanagh, S., Morrison, L., Fogarty, A., Cormican, M., Dockery, P., Prendergast, M., Rowan, N. and Morris, D., 2017. Silver nanoparticles in the environment: sources, detection and ecotoxicology. Sci. Total Environ. 575, 231-246.
- Messina, F., Marchisio, D.L. and Sethi, R., 2015. An extended and total flux normalized correlation equation for predicting single-collector efficiency. J. Colloid Interface Sci. 446, 185-193.
- Molnar, I.L., Pensini, E., Asad, M.A., Mitchell, C.A., Nitsche, L.C., Pyrak-Nolte, L.J., Miño, G.L. and Krol, M.M., 2019. Colloid transport in porous media: a review of classical mechanisms and emerging topics. Transport in Porous Media.
- Neukum, C., 2018. Transport of silver nanoparticles in single fractured sandstone. J. Contam. Hydrol. 209, 61-67.
- Nowack, B., Krug, H.F. and Height, M., 2011. 120 years of nanosilver history: implications for policy makers. Environ. Sci. Technol. 45(4), 1177-1183.
- Park, C.M., Heo, J., Her, N., Chu, K.H., Jang, M. and Yoon, Y., 2016. Modeling the effects of surfactant, hardness, and natural organic matter on deposition and mobility of silver nanoparticles in saturated porous media. Water Res. 103, 38-47.
- Rabinovich, Y.I., Adler, J.J., Ata, A., Singh, R.K. and Moudgil, B.M., 2000. Adhesion between nanoscale rough surfaces: Ii. Measurement and comparison with theory. J. Colloid Interface Sci. 232(1), 17-24.

- Rasmuson, A., Pazmino, E., Assemi, S. and Johnson, W.P., 2017. Contribution of nano- to microscale roughness to heterogeneity: closing the gap between unfavorable and favorable colloid attachment conditions. Environ. Sci. Technol. 51(4), 2151-2160.
- Rasmuson, A., VanNess, K., Ron, C.A. and Johnson, W.P., 2019. Hydrodynamic versus surface interaction impacts of roughness in closing the gap between favorable and unfavorable colloid transport conditions. Environ. Sci. Technol. 53(5), 2450-2459.
- Rezvani, E., Rafferty, A., McGuinness, C. and Kennedy, J., 2019. Adverse effects of nanosilver on human health and the environment. Acta Biomater. 94, 145-159.
- Ron, C.A., VanNess, K., Rasmuson, A. and Johnson, W.P., 2019. How nanoscale surface heterogeneity impacts transport of nano- to micro-particles on surfaces under unfavorable attachment conditions. Environ Sci Nano. 6(6), 1921-1931.
- Shellenberger, K. and Logan, B.E., 2002. Effect of molecular scale roughness of glass beads on colloidal and bacterial deposition. Environ. Sci. Technol. 36(2), 184-189.
- Shen, C., Bradford, S.A., Li, T., Li, B. and Huang, Y., 2018. Can nanoscale surface charge heterogeneity really explain colloid detachment from primary minima upon reduction of solution ionic strength? J. Nanopart. Res. 20(6), 165.
- Shen, C., Huang, Y., Li, B. and Jin, Y., 2010. Predicting attachment efficiency of colloid deposition under unfavorable attachment conditions. Water Resour. Res. 46(11), W11526.
- Shen, C., Jin, Y., Zhuang, J., Li, T. and Xing, B., 2019. Role and importance of surface heterogeneities in transport of particles in saturated porous media. Crit. Rev. Environ. Sci. Technol., 1-86.
- Shen, C., Wang, L.-P., Li, B., Huang, Y. and Jin, Y., 2012. Role of surface roughness in chemical detachment of colloids deposited at primary energy minima. Vadose Zone J. 11(1), 59-75.

- Shen, C.Y., Li, B.G., Chao, W., Huang, Y.F. and Yan, J., 2011. Surface roughness effect on deposition of nano- and micro-sized colloids in saturated columns at different solution ionic strengths. Vadose Zone J. 10(3), 1071-1081.
- Suresh, L. and Walz, J.Y., 1996. Effect of surface roughness on the interaction energy between a colloidal sphere and a flat plate. J. Colloid Interface Sci. 183(1), 199-213.
- Torkzaban, S. and Bradford, S.A., 2016. Critical role of surface roughness on colloid retention and release in porous media. Water Res. 88, 274-284.
- Torkzaban, S., Bradford, S.A. and Walker, S.L., 2007. Resolving the coupled effects of hydrodynamics and dlvo forces on colloid attachment in porous media. Langmuir 23(19), 9652-9660.
- Tufenkji, N. and Elimelech, M., 2004. Correlation equation for predicting single-collector efficiency in physicochemical filtration in saturated porous media. Environ. Sci. Technol. 38(2), 529-536.
- Vance, M.E., Todd, K., P, V.E., P, M.S., F, H.M., David, R. and S, H.M., 2015. Nanotechnology in the real world: redeveloping the nanomaterial consumer products inventory. Beilstein J Nanotechnol. 6, 1769-1780.
- Verwey, E.J.W. and Overbeek, J.T.G., 1948. Theory of the stability of lyophobic colloids, Elsevier, Amsterdam, The Netherlands.
- Wang, H., Zhang, W., Zeng, S., Shen, C., Jin, C. and Huang, Y., 2019. Interactions between nanoparticles and fractal surfaces. Water Res. 151, 296-309.
- Wang, M., Gao, B. and Tang, D., 2016. Review of key factors controlling engineered nanoparticle transport in porous media. J. Hazard. Mater. 318, 233-246.
- Yao, K.-M., Habibian, M.T. and O'Melia, C.R., 1971. Water and waste water filtration. Concepts and applications. Environ. Sci. Technol. 5(11), 1105-1112.

- Yu, S.J., Yin, Y.G. and Liu, J.F., 2013. Silver nanoparticles in the environment. Environ Sci Process Impacts 15(1), 78-92.
- Zhang, M., Bradford, S.A., Šimůnek, J., Vereecken, H. and Klumpp, E., 2016. Do goethite surfaces really control the transport and retention of multi-walled carbon nanotubes in chemically heterogeneous porous media? Environ. Sci. Technol. 50(23), 12713-12721.

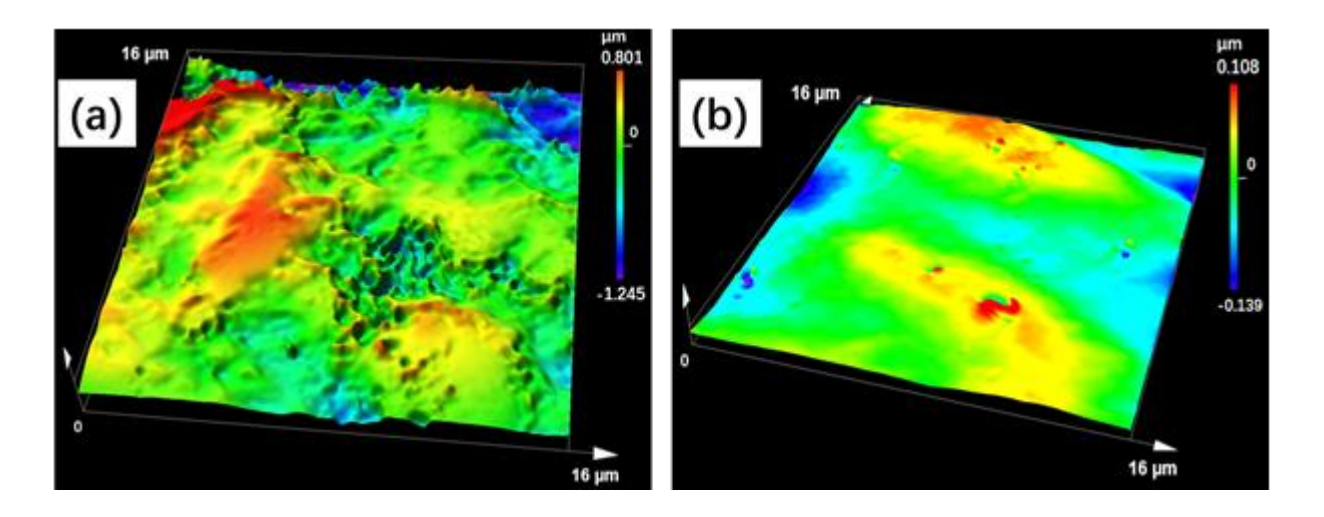


Fig. 1. Laser scanning confocal microscope images of rough sand (a) and relatively smooth sand (b) used for column experiments.

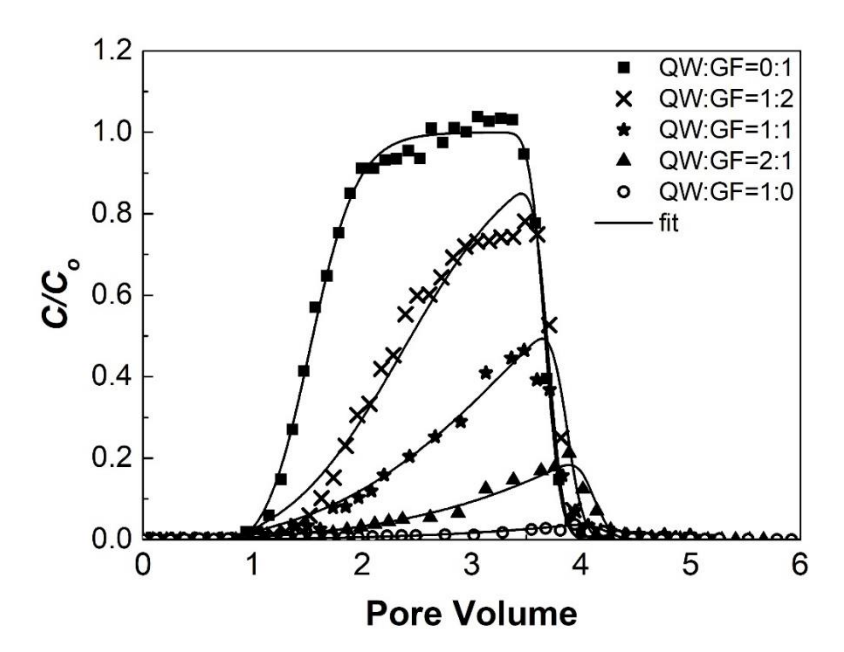


Fig.2. Observed and fitted breakthrough curves of AgNPs in various mixture ratios of rough and relatively smooth sand (QW and GF denote rough and relatively smooth sand, respectively) when the IS=5 mM KNO<sub>3</sub> and pH=6.5. Lines were fitted results.

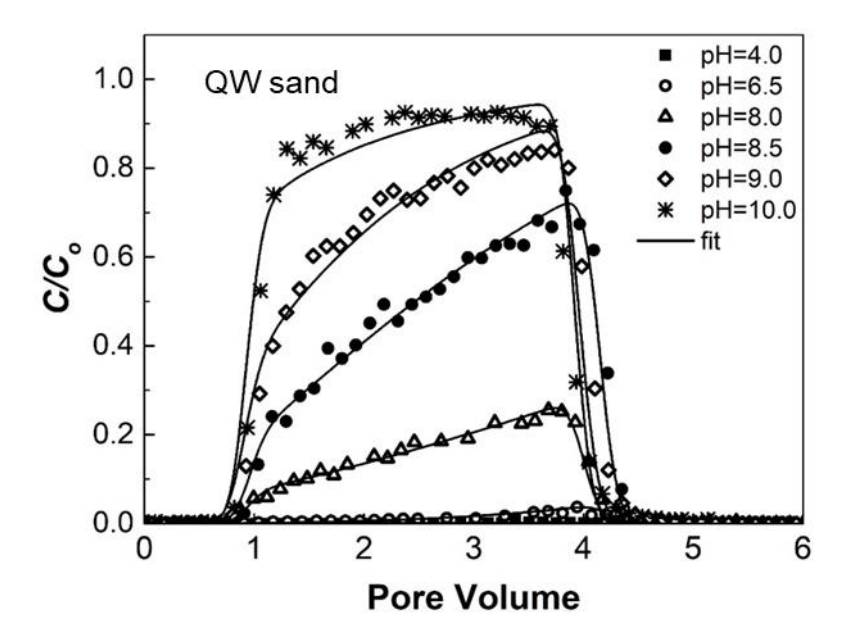


Fig.3. Observed and fitted breakthrough curves of AgNPs under various pH values in rough sand (QW denotes rough sand) when the IS=5 mM KNO<sub>3</sub>. Lines were fitted results.

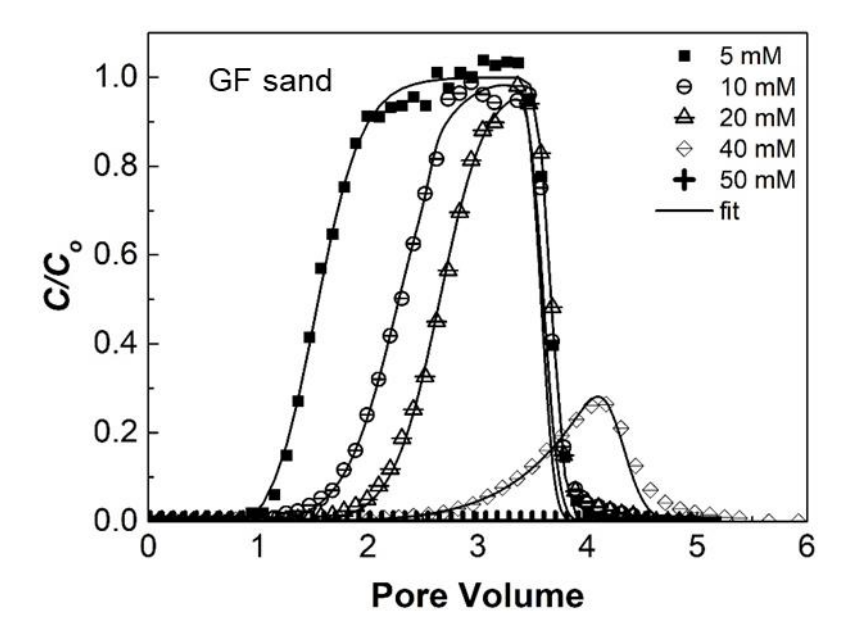


Fig. 4. Observed and fitted breakthrough curves of AgNPs under various ionic strength in relatively smooth sand (GF denotes relatively smooth sand) when the pH=6.5. Lines were fitted results.

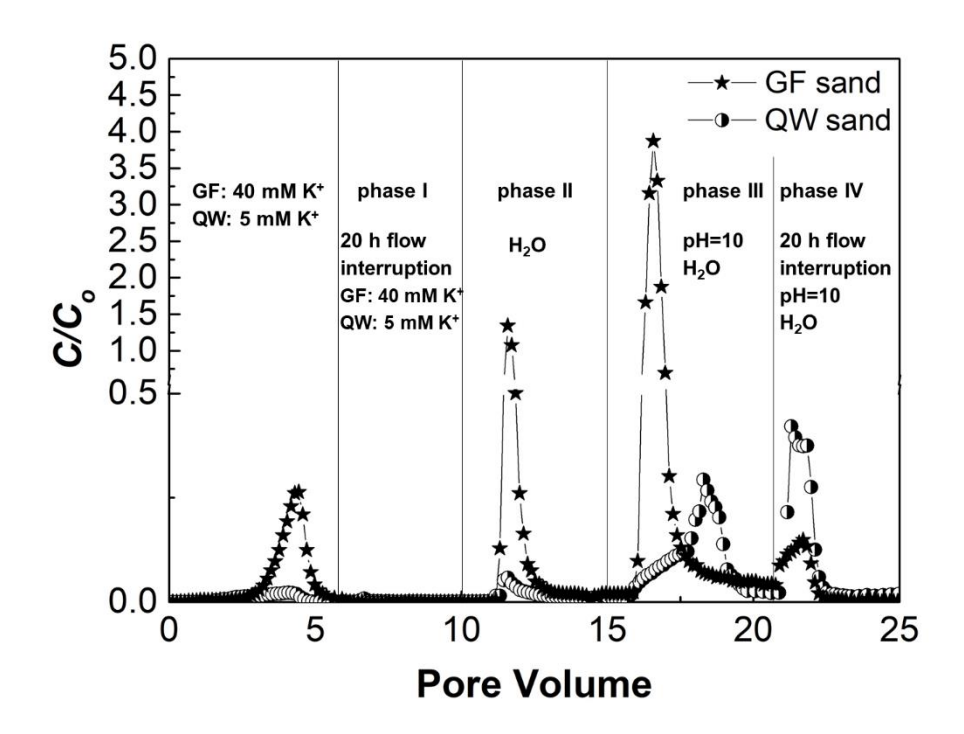


Fig. 5. AgNP release from relatively smooth and rough sand (QW and GF denote rough and relatively smooth sand, respectively). AgNP retention occurred at 40 and 5 mM KNO<sub>3</sub>, respectively; release of AgNPs was initiated by 20 h interruption flow with 40 and 5 mM KNO<sub>3</sub> (phase I, pH=6.5), eluting with ultrapure water (phase II, pH=6.5; phase III, pH=10) and 20 h interruption flow with ultrapure water (phase IV, pH=10).

Table 1. Experimental Parameters and Fitted/Calculated Values ( $k_1$ ,  $S_{\text{max}}/C_0$ , and  $S_f$ ) of AgNP Transport under Various Experimental Conditions.

	Exp. Name	$M_{ m QW}$	IS mM	рН	$M_{\it eff}$ , %	$k_1$ , min <sup>-1</sup>	$S_{\rm max}/C_{\rm o}$ , cm <sup>3</sup> $g^{-1}$	S <sub>f</sub> , % BET	S <sub>f</sub> , % Geometric	$R^2$
Fig. 2	QW:GF=0:1	0.00	5	6.5	79.2	0.346	0.166	0.236	0.645	0.997
	QW:GF=1:2	0.33	5	6.5	45.3	0.409	0.443	0.445	1.787	0.966
	QW:GF=1:1	0.50	5	6.5	21.2	0.485	0.713	0.584	2.722	0.949
	QW:GF=2:1	0.67	5	6.5	8.5	0.741	0.964	0.669	3.549	0.979
	QW:GF=1:0	1.00	5	6.5	1.5	1.026	1.467	0.800	5.279	0.951
Fig. 3	pH=4.0	1.00	5	4.0	0.2	1.378	2.199	1.272	8.393	0.443
	pH=6.5	1.00	5	6.5	1.5	1.026	1.467	0.800	5.279	0.951
	pH=8.0	1.00	5	8.0	17.8	0.383	1.195	0.693	4.571	0.981
	pH=8.5	1.00	5	8.5	51.2	0.234	0.424	0.252	1.659	0.984
	pH=9.0	1.00	5	9.0	71.8	0.148	0.233	0.145	0.955	0.977
	pH=10.0	1.00	5	10.0	86.3	0.049	0.114	0.069	0.453	0.981
Fig. 4	5 mM	0.00	5	6.5	79.2	0.346	0.166	0.236	0.645	0.997
	10 mM	0.00	10	6.5	49.6	0.751	0.436	0.880	2.401	0.970
	20 mM	0.00	20	6.5	39.7	1.091	0.537	0.846	2.310	0.969
	40 mM	0.00	40	6.5	8.8	1.313	0.767	1.164	3.177	0.965
	50 mM	0.00	50	6.5	0.0	1.622	1.947	2.953	8.060	0.406
Fig. S5	pH 6.5	0.00	50	6.5	0.0	1.622	1.947	2.953	8.060	0.406
	pH 8.0	0.00	50	8.0	78.1	0.632	0.183	0.378	1.031	0.967
					$M_{\it eff}$	$M_{ m I}$	$M_{\mathrm{II}}$	$M_{\rm III}$	$M_{\rm IV}$	$M_{ m V}$
Fig.5	GF sand	0	5	6.5	8.8	0.1	18.2	70.6	5.0	< 0.1
	QW sand	1.00	40	6.5	1.3	0.1	2.1	14.7	12.8	5.2

QW and GF denote rough and relatively smooth sand, respectively;  $M_{\rm QW}$ , mass percentage of rough QW sand in columns;  $M_{\rm eff}$ , the mass percentages of AgNPs recovered from effluent;  $M_{\rm I}-M_{\rm V}$ , the mass percentages of AgNPs recovered from phase I – V in release experiments;  $k_{\rm I}$ , the first-order retention coefficient;  $S_{\rm max}/C_{\rm o}$ , normalized maximum solid phase concentration of deposited NPs;  $S_f$ , the fraction of the grain surface area that contributes to AgNP retention, BET and geometric denote  $S_f$  calculation based on BET measurements and geometric estimates, respectively;  $R^2$ , Pearson's correlation coefficient. Constant Darcy velocity= 0.7 cm min<sup>-1</sup> and  $C_0$ =10 mg L<sup>-1</sup> were employed in all experiments.

# **Supporting Information**

# Introduction

The supplementary information provides a brief description and discussion of: (i) characterization of quartz sand; (ii) interaction energy calculations (S1); (iii) mathematical modeling (S2); (iv) SEM images of QW sand and GF sand (Fig. S1); (v) interaction energy profiles for different IS without (a) and with (b) steric interactions (Fig. S2); (vi) correlation of silver nanoparticle (AgNP) mass recovery in the effluent ( $M_{eff}$ ),  $k_1$ , and  $S_{max}/C_o$  with the mass percentage of rough QW sand and pH (Fig. S3); (vii) SEM images of AgNPs retained on QW and GF sand surfaces (Fig. S4); (viii) effect of pH in relatively smooth GF sand (Fig S5); (ix) zeta potentials (AgNPs and quartz sand) and the hydrodynamic diameters of AgNPs for experimental solution chemistries and calculated interaction energy parameters (Table S1); (x) surface roughness parameters measured by laser scanning confocal microscope (Table S2); (xi) influence of surface roughness on interaction energy parameters for AgNP-Sand interaction when pH=4 and 10 and the IS=5 mM (Table S3).

#### S1. Characterization of quartz sand

Scanning electron microscopes (SEM, Nova NanoSEM 450, FEI Company, The Netherlands and SU8220, Hitachi, Japan) were employed to obtain the general surface structure and the surface roughness information for the two sands. In addition, surface roughness of the sands was quantified using a laser scanning confocal microscope (LSCM, Olympus LEXT OLS5000, Japan). Four small areas with  $16 \times 16 \, \mu m$  were randomly selected to obtain the area roughness parameters such as average roughness ( $S_a$ ), root mean square roughness ( $S_q$ ), maximum roughness ( $S_z$ ), and (root mean square gradient (Sdq). The sizes of the sands were measured by a laser particle size analyzer (Mastersizer 3000, Malvern Panalytical, U.K.) to get the information of  $d_{10}$ ,  $d_{50}$ , and  $d_{90}$ . The

specific surface area was determined using krypton adsorption (Quantachrome instruments, U.S.) and calculated by the multipoint Brunauer-Emmett-Teller (BET) method. Chemical properties of the sand surfaces were obtained by analyzing the amount of Al, Fe, Mg, and Ca by inductively coupled plasma-mass spectrometry after boiling the sand in HNO<sub>3</sub> for 2 h following the purification processes described in section 2.2 in the main manuscript. To better compare the surface properties of the sand, the sand surface charge was determined from streaming potential measurements by SurPASS electrokinetic analyzer (Anton Paar, Graz, Austria) to avoid damage of the grain surface. Zeta potentials of the sands in all the background solution chemistries as for transport and release experiments were investigated.

#### **S2.** Interaction energy calculations

The AgNP-sand interaction energy was calculated using a sphere-plate assumption (Derjaguin and Landau 1941, Verwey and Overbeek 1948). The value of the total interaction energy ( $\Phi$ ) was considered to be the sum of electrostatic, van der Waals, steric, and Born repulsion interaction energies:

$$\Phi(h) = \Phi^{sl}(h) + \Phi^{vdw}(h) + \Phi^{st}(h) + \Phi^{Born}(h)$$
[S1]

where  $\Phi$  [ML<sup>2</sup>T<sup>-2</sup>, where M, L, and T denote units of mass, length, and time, respectively],  $\Phi^{sl}$  [ML<sup>2</sup>T<sup>-2</sup>],  $\Phi^{vdw}$  [ML<sup>2</sup>T<sup>-2</sup>],  $\Phi^{st}$  [ML<sup>2</sup>T<sup>-2</sup>], and  $\Phi^{Born}$  [ML<sup>2</sup>T<sup>-2</sup>] are the total, electrostatic, van der Waals, steric, and Born interaction energies, respectively, and h [L] is the separation distance from the center of the AgNP to the solid surface. The value of  $\Phi^{el}$  was determined using the constant surface potential interaction expression of Hogg et al. (1966) for a sphere-plate interaction as:

$$\Phi^{el}(h) = \pi \varepsilon \varepsilon_o r_c \left\{ 2\zeta_1 \zeta_2 \ln \left[ \frac{1 + \varepsilon \kappa p(-\kappa h)}{1 - \varepsilon \kappa p(-\kappa h)} \right] + \left( {\zeta_1}^2 + {\zeta_2}^2 \right) \ln \left[ 1 - \varepsilon \kappa p(-2\kappa h) \right] \right\} \quad [S2]$$

where  $\varepsilon$  (dimensionless) is the dielectric constant of the medium,  $\varepsilon_o$  [M<sup>-1</sup>L<sup>-3</sup>T<sup>4</sup>A<sup>-2</sup>, where A denotes ampere] is the permittivity in a vacuum,  $r_c$  [L] is the radius of a nanoparticle,  $\zeta_1$  is the mean zeta potential of the AgNP,  $\zeta_2$  is the mean zeta potential of the aquifer material, and  $\kappa$  [L<sup>-1</sup>] is the Debye-Huckel parameter. The value of  $\Phi^{vdw}$  for a sphere-plate interaction was determined using the expression by Gregory (1981) as:

$$\Phi^{vdW}(h) = -\frac{A_{123} r_c}{6h} \left[ 1 + \frac{14h}{\lambda} \right]^{-1}$$
 [S3]

where  $A_{123}$  [ML<sup>2</sup>T<sup>-2</sup>] is the Hamaker constant taken as  $5.3 \times 10^{-20}$  J (Bhattacharya et al. 2008), and  $\lambda$  is a characteristic wavelength that was taken as 100 nm (Gregory 1981). The value of  $\Phi^{Born}$  was calculated from Ruckenstein and Prieve (1976) as:

$$\Phi^{Born}(h) = \frac{A_{123} \sigma_c^6}{7560} \left[ \frac{8r_c + h}{(2r + 7)^7} + \frac{6r_c - h}{h^7} \right]$$
 [S4]

The collision diameter,  $\sigma_c$ , was taken as 0.26 nm in order to achieve a primary minimum depth at 0.157 nm, a commonly accepted distance of closest approach (Van Oss 1994). To take into account steric interaction (due to the presence of surfactant coating on AgNP surface) for the total interaction energies, the estimation of the steric interaction between AgNPs and quartz sand (uncoated flat surface) is determined using the expression as Petosa et al. (2010):

$$F^{st}(h) = 2\pi r_c \left(\frac{k_B T_K}{\sigma^3}\right) \left\{\frac{8L_c}{5} \left[\left(\frac{2L_c}{h}\right)^{5/4} - 1\right] + \frac{8L_c}{7} \left[\left(\frac{h}{2L_c}\right)^{7/4} - 1\right]\right\}$$

$$\Phi^{st}(h) = -\int_{\infty}^{h} F^{st}(h) dh$$
 [S5]

where  $F^{st}$  [MLT<sup>-2</sup>] is the steric force,  $k_B$  is the Boltzmann constant (=1.38×10<sup>-23</sup> J K<sup>-1</sup>),  $T_K$  is the absolute temperature,  $\sigma$  [L] is the distance between the surfactant chains on the surface, and  $L_c$  [L] is the thickness of the coating layer covering the nanoparticles. The value of  $\sigma$  and L were taken to be 5 nm (Hwang et al. 2018) and 10 nm (Liang et al. 2013), respectively. The steric interaction was neglected in Eq. [S1] unless otherwise noted.

Nanoscale roughness has been demonstrated to significantly influence the prediction for interaction energy (Huang et al. 2010, Shen et al. 2012, Torkzaban and Bradford 2016, Zhang et al. 2016). In this study, the sand surface was assumed to contain a nanoscale roughness fraction ( $f_{sr}$ ) with a height equal to  $h_{sr}$ =37 nm (Han et al. 2016, Rasmuson et al. 2017). Similarly, the AgNP surface contained a nanoscale roughness fraction ( $f_{cr}$ ) with a height equal to  $h_{cr}$ =10 nm (Liang et al. 2013). The interaction energy between the rough AgNP and sand ( $\Phi_r$ , MLT<sup>-1</sup>) was determined as a linear combination of interaction energies for the various nanoscale roughness components as Bradford et al. (2017):

$$\Phi_r(h) = a_{r1}\Phi(h + h_{sr} + h_{cr}) + a_{r2}\Phi(h + h_{sr}) + a_{r3}\Phi(h + h_{cr}) + a_{r4}\Phi(h)$$
 [S6]

where  $a_{r1}$  [-],  $a_{r2}$  [-],  $a_{r3}$  [-], and  $a_{r4}$  [-] are constants that determine the contributions of the various possible roughness combinations that are equal to:

$$a_{r1} = (1 - f_{sr})(1 - f_{cr})$$

$$a_{r2} = (1 - f_{sr})f_{cr}$$

$$a_{r3} = f_{sr}(1 - f_{cr})$$

$$a_{r4} = f_{sr}f_{cr}$$
[S7]

It should be mentioned that h in Eq. [S6] is the separation distance at a height  $h_{sr}$  from the solid water interface to the leading face of the AgNPs at a height  $h_{cr}$ , such that h is always greater than 0 and the roughness on the AgNP and solid do not overlap. In this case, the lateral components of the interaction energy are insignificant or cancel out.

All interaction energies were made dimensionless by dividing by the product of the Boltzmann constant ( $k_{\rm B} = 1.38 \times 10^{-23}$  J K<sup>-1</sup>) and the absolute temperature (T<sub>K</sub>).

## S3. Transport model

Experimental BTCs were inversely fitted to AgNP transport model using Version 4.14 of the HYDRUS-1D computer code (Šimůnek et al. 2008) to obtain the parameters of  $k_1$  and  $S_{\text{max}}$ , which represent the first-order retention coefficient and the maximum solid phase concentration of deposited AgNPs, respectively. Transport of AgNPs in the aqueous phase was described using the advection-dispersion equation that includes an exchange term to/from the aqueous and the solid phases:

$$\frac{\partial(\theta_w c)}{\partial t} + \frac{\partial(\rho_b s)}{\partial t} = \frac{\partial}{\partial z} \left( \theta_w D \frac{\partial c}{\partial z} \right) - \frac{\partial(qc)}{\partial z}$$
 [S8]

where  $\theta_w$  [–] is the volumetric water content, C [N<sub>c</sub> L<sup>-3</sup>, N<sub>c</sub> and L denote the number of AgNPs and units of length, respectively] is the aqueous phase AgNP concentration, t is time [T], z [L] is the distance from the column inlet,  $\rho_b$  [M L<sup>-3</sup>, M denote units of mass] is the soil bulk density, S [N<sub>c</sub> M<sup>-1</sup>] is the solid phase AgNP concentration, D [L<sup>2</sup>T<sup>-1</sup>] is the hydrodynamic dispersion coefficient, q [L T<sup>-1</sup>] is the Darcy water flux. In Eq. [S8], the second term on the left-hand side is used to describe AgNP retention on the solid phase, and the first and second terms on the right-hand side account for the dispersive and advective fluxes of AgNPs, respectively.

The solid phase mass balance equation is given in this work as:

$$\frac{\partial(\rho_b S)}{\partial t} = \theta_w k_1 \psi C \tag{S9}$$

where  $k_1$  [T<sup>-1</sup>] is the first-order retention coefficient,  $\psi$  [-] is a dimensionless function to account for time-dependent blocking/filling of retention sites using a Langmuirian approach (Deshpande and Shonnard 1999) and it is given in Eq. [S9] as:

$$\psi = 1 - \frac{s}{s_{max}} \tag{S10}$$

where  $S_{\text{max}}$  [N<sub>c</sub> M<sup>-1</sup>] is the maximum solid phase concentration of deposited AgNPs. Values of the Darcy velocity (q), porosity  $(\theta)$ , bulk density  $(\rho)$ , and dispersivity  $(\lambda)$  were determined from available experimental information and tracer experiments. Other model parameters were

determined by optimization to AgNP breakthrough curves using the Levenberg-Marquardt nonlinear least squares fitting routine in HYDRUS-1D (Šimůnek et al. 2008).

Additionally, based on the fitted  $S_{\text{max}}$  obtained from numerical simulations described above, the fraction of the solid surface area that is available for AgNP deposition ( $S_f$ ) was calculated as Kim et al. (2009):

$$S_f = \frac{A_c \rho_b S_{max}}{(1 - \gamma) A_s}$$
 [S11]

where  $A_c$  (L<sup>2</sup> N<sup>-1</sup>) is the cross-section area per AgNP (a value of 15 nm was used based on TEM measurement),  $\gamma$  is the porosity of a monolayer packing of AgNPs on the solid surface and a value of 0.5 for  $\gamma$  was applied for all the calculations (Johnson and Elimelech 1995), and  $A_s$  (L<sup>-1</sup>) is the solid surface area per unit volume.  $A_s$  was calculated based on both BET measurements and geometric estimates for comparison. An equation of 6 \* (1-porosity)/d<sub>50</sub> was used for geometric estimates (Zhang et al. 2016).

## References

Bhattacharya, S.N., Kamal, M.R. and Gupta, R.K., 2008. Polymeric nanocomposites - theory and practice, Hanser Publishers.

Bradford, S.A., Kim, H., Shen, C., Sasidharan, S. and Shang, J., 2017. Contributions of nanoscale roughness to anomalous colloid retention and stability behavior. Langmuir 33(38), 10094-10105.

Derjaguin, B. and Landau, L., 1941. Theory of the stability of strongly charged lyophobic sols and of the adhesion of strongly charged particles in solutions of electrolytes. Acta Physicochimica U.S.S.R 14, 633-662.

Deshpande, P.A. and Shonnard, D.R., 1999. Modeling the effects of systematic variation in ionic strength on the attachment kinetics of pseudomonas fluorescens uper-1 in saturated sand columns. Water Resour. Res. 35(5), 1619-1627.

Gregory, J., 1981. Approximate expressions for retarded van der waals interaction. J. Colloid Interface Sci. 83(1), 138-145.

- Han, Y., Hwang, G., Kim, D., Bradford, S.A., Lee, B., Eom, I., Kim, P.J., Choi, S.Q. and Kim, H., 2016. Transport, retention, and long-term release behavior of zno nanoparticle aggregates in saturated quartz sand: Role of solution ph and biofilm coating. Water Res. 90(Supplement C), 247-257.
- Hogg, R., Healy, T.W. and Fuerstenau, D.W., 1966. Mutual coagulation of colloidal dispersions. Trans. Faraday Soc. 62, 1638-1651.
- Huang, X., Bhattacharjee, S. and Hoek, E.M.V., 2010. Is surface roughness a "scapegoat" or a primary factor when defining particle—substrate interactions? Langmuir 26(4), 2528-2537.
- Hwang, G., Gomez-Flores, A., Bradford, S.A., Choi, S., Jo, E., Kim, S.B., Tong, M. and Kim, H., 2018. Analysis of stability behavior of carbon black nanoparticles in ecotoxicological media: Hydrophobic and steric effects. Colloids Surf. Physicochem. Eng. Aspects 554, 306-316.
- Johnson, P.R. and Elimelech, M., 1995. Dynamics of colloid deposition in porous media: Blocking based on random sequential adsorption. Langmuir 11(3), 801-812.
- Kim, H.N., Bradford, S.A. and Walker, S.L., 2009. Escherichia coli o157:H7 transport in saturated porous media: Role of solution chemistry and surface macromolecules. Environ. Sci. Technol. 43(12), 4340-4347.
- Liang, Y., Bradford, S.A., Simunek, J., Vereecken, H. and Klumpp, E., 2013. Sensitivity of the transport and retention of stabilized silver nanoparticles to physicochemical factors. Water Res. 47(7), 2572-2582.
- Petosa, A.R., Jaisi, D.P., Quevedo, I.R., Elimelech, M. and Tufenkji, N., 2010. Aggregation and deposition of engineered nanomaterials in aquatic environments: Role of physicochemical interactions. Environ. Sci. Technol. 44(17), 6532-6549.
- Rasmuson, A., Pazmino, E., Assemi, S. and Johnson, W.P., 2017. Contribution of nano- to microscale roughness to heterogeneity: Closing the gap between unfavorable and favorable colloid attachment conditions. Environ. Sci. Technol. 51(4), 2151-2160.
- Ruckenstein, E. and Prieve, D.C., 1976. Adsorption and desorption of particles and their chromatographic-separation. Aiche J 22(2), 276-283.
- Shen, C., Lazouskaya, V., Jin, Y., Li, B., Ma, Z., Zheng, W. and Huang, Y., 2012. Coupled factors influencing detachment of nano- and micro-sized particles from primary minima. J. Contam. Hydrol. 134-135, 1-11.
- Šimůnek, J., Genuchten, M.T.v. and Šejna, M., 2008. Development and applications of the hydrus and stanmod software packages, and related codes. Vadose Zone J. 7(2), 587-600.

- Torkzaban, S. and Bradford, S.A., 2016. Critical role of surface roughness on colloid retention and release in porous media. Water Res. 88, 274-284.
- Van Oss, C., 1994. Relation between the hamaker constant and the apolar surface tension component. In: Interfacial forces in aqueous media. 154-155. Van oss cj, editor. New york: Marcel dekker.
- Verwey, E.J.W. and Overbeek, J.T.G., 1948. Theory of the stability of lyophobic colloids, Elsevier, Amsterdam.
- Zhang, M., Bradford, S.A., Šimůnek, J., Vereecken, H. and Klumpp, E., 2016. Do goethite surfaces really control the transport and retention of multi-walled carbon nanotubes in chemically heterogeneous porous media? Environ. Sci. Technol. 50(23), 12713-12721.

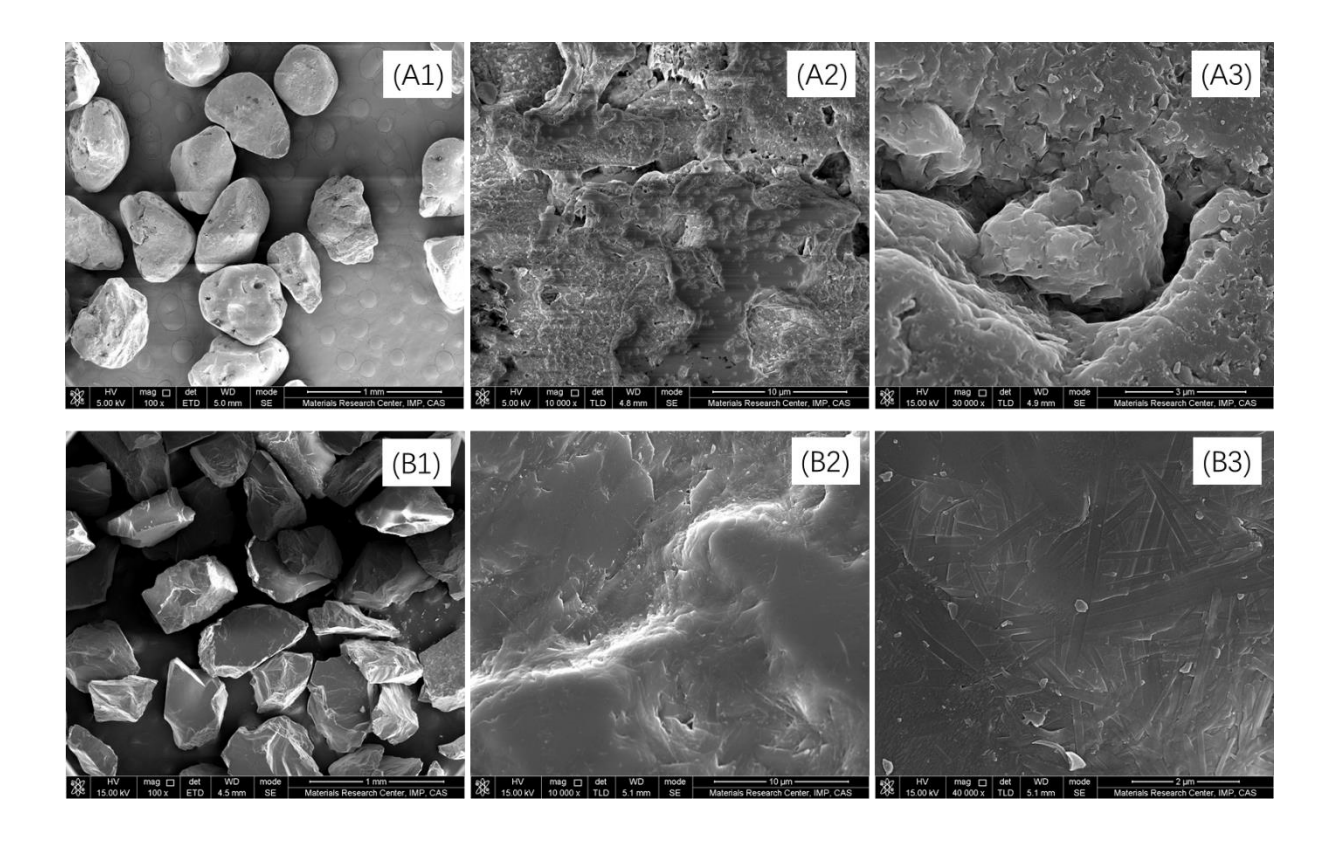


Fig. S1. Scanning electron microscope (SEM) images of rough sand (A) and relatively smooth sand (B).

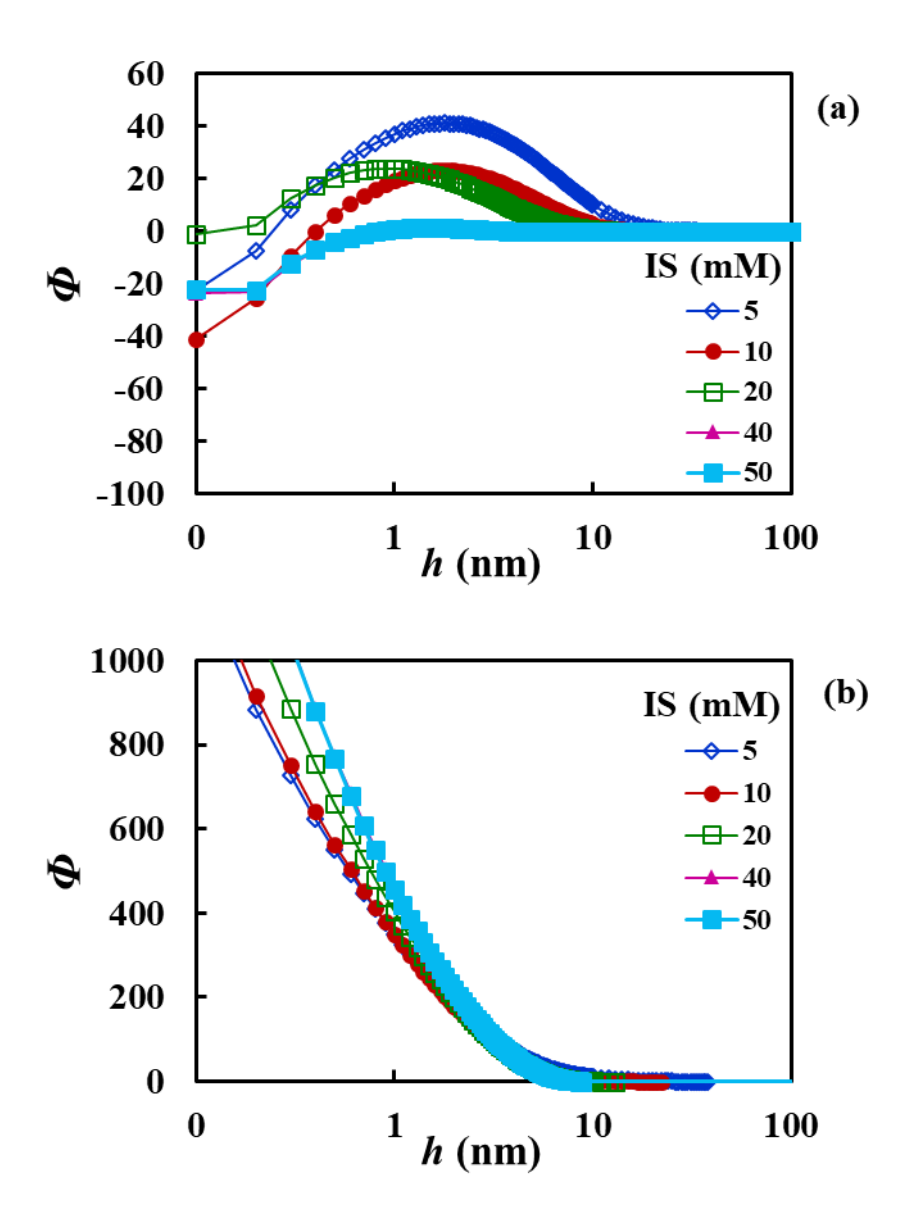


Fig. S2. Interaction energy profiles for different IS without (a) and with (b) steric interactions

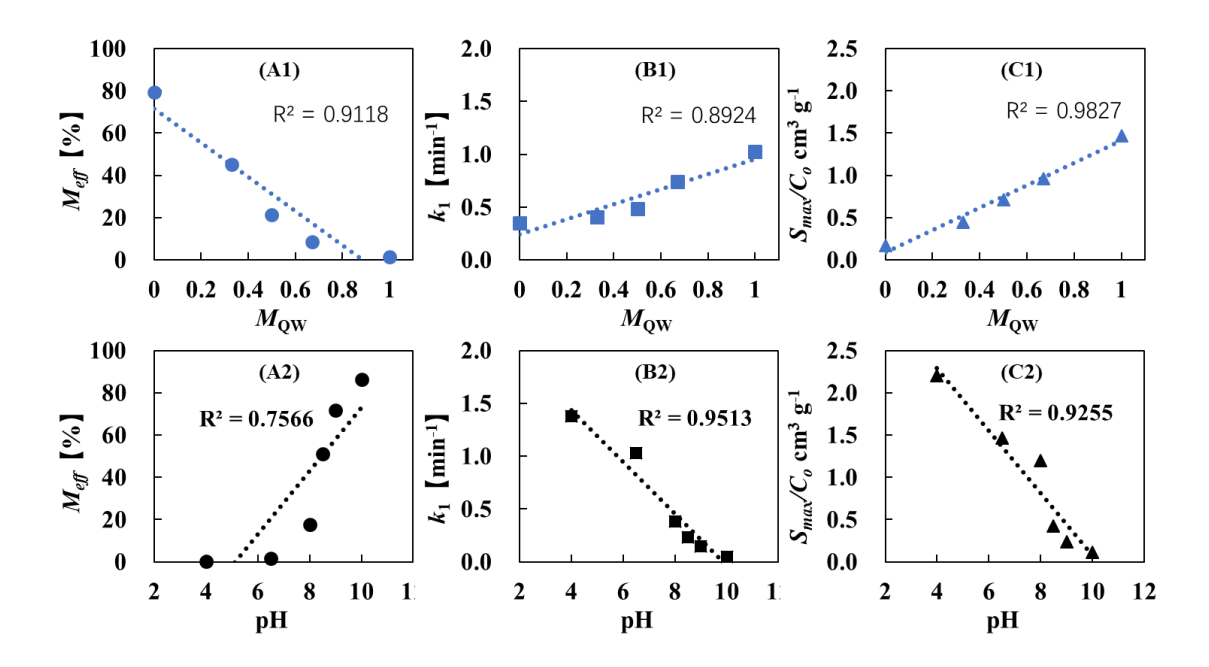


Fig. S3. Correlation of AgNP mass recovery in the effluent ( $M_{eff}$ ) (A) and the fitted parameters of  $k_1$  (B) and  $S_{max}/C_o$  (C) with the mass percentage of rough sand ( $M_{QW}$ ) and solution pH. QW denotes rough sand.

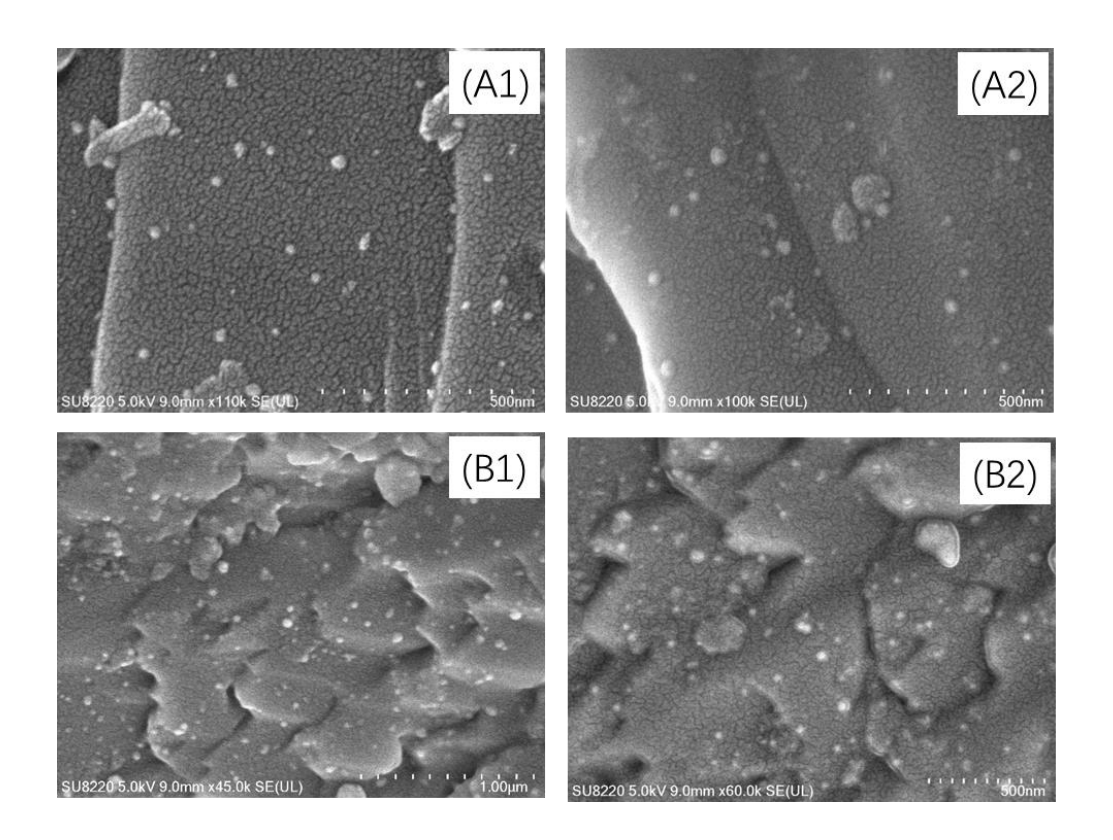


Fig. S4. SEM images of retained AgNPs on relatively smooth (A) sand and rough sand (B) surfaces. Bright dots are AgNPs.

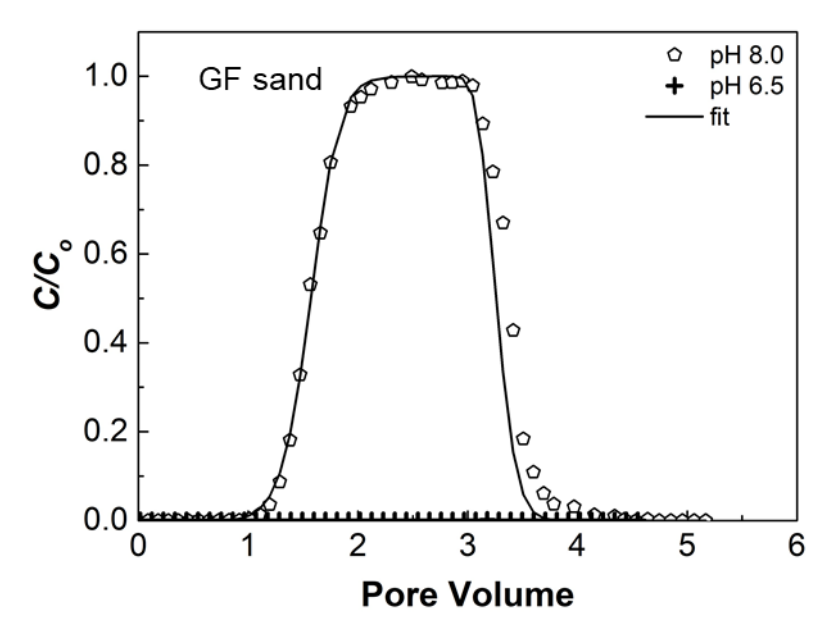


Fig.S5. Observed and fitted breakthrough curves of AgNPs under pH of 6.5 and 8.0 at 50 mM KNO<sub>3</sub> in relatively smooth sand (GF denotes smooth sand). Lines were fitted results. Other experimental conditions were the same: input concentration of AgNPs, 10 mg/L; Darcy velocity, 0.7

Table S1. Zeta potentials (AgNPs and quartz sand) and the hydrodynamic diameters of AgNPs ( $d_p$ ) for experimental solution chemistries and calculated interaction energy parameters for AgNP-Sand interaction obtained from DLVO calculations: without consideration of steric interaction and surface roughness

	YG 5 N 63	**	d <sub>p</sub> , nm	Zeta potential, mV		- Φ <sub>max</sub> [-	$\Delta \Phi_d$ [-	$\Phi_{ m lmin}$ [-
	IS [mM]	pН		AgNPs	sand	- • max [		]
	5	4.0	$110.7 \pm 3.2$	$-5.9 \pm 1.9$	$-29.0 \pm 0.8$	3.3	61.9	-58.6
Rough	5	6.5	$83.6 \pm 5.4$	$-22.6 \pm 1.6$	$-48.5 \pm 1.0$	39.4	37.3	2.1
sand	5	8.0	$75.2 \pm 6.9$	$-22.8 \pm 2.2$	$-52.3 \pm 1.7$	36.7	41.9	-5.1
(QW)	5	8.5	$71.8 \pm 3.9$	$-24.2 \pm 0.3$	$-53.4 \pm 1.6$	39.4	38.1	1.3
	5	9.0	$71.4 \pm 10.8$	$-25.8 \pm 1.7$	$-54.9 \pm 1.8$	44.3	36.3	8.0
	5	10.0	$62.9 \pm 9.8$	$-30.4 \pm 2.4$	$-57.3 \pm 3.8$	53.1	24.9	28.2
	5	6.5	$83.6 \pm 5.4$	-22.6 ± 1.6	$-57.4 \pm 1.4$	41.0	63.7	-22.7
Smooth	10	6.5	$88.4 \pm 8.5$	$-16.7 \pm 0.6$	$-51.0 \pm 4.4$	23.1	64.1	-41.0
sand	20	6.5	$101.5\pm3.6$	$-17.2 \pm 3.3$	$-36.8 \pm 6.5$	23.7	25.1	-1.4
(GF)	40	6.5	$123.0\pm1.5$	$-7.4 \pm 1.1$	$-18.8 \pm 9.8$	1.9	25.4	-23.5
	50	6.5	$122.2 \pm 5.0$	$-7.4 \pm 1.0$	$-17.7 \pm 8.4$	1.2	23.7	-22.4

 $\Phi_{max}$ , energy barrier height;  $\Phi_{lmin}$ , depth of the primary minimum;  $\Delta\Phi_d$ , the energy barrier to detachment from the primary minimum ( $\Delta\Phi_d = \Phi_{max} - \Phi_{lmin}$ )

Table S2. Measured physicochemical parameters of rough sand and relatively smooth sand

	Parameters	QW sand	GF sand	
	Sa, average roughness, nm	$418 \pm 150$	78 ± 41	
	$S_{\rm q}$ , root mean square roughness, nm	$524 \pm 166$	$93 \pm 49$	
	$S_z$ , maximum roughness, nm	$3706 \pm 665$	$733 \pm 278$	
Surface	Sdq, root mean square gradient, nm	$729 \pm 165$	$153 \pm 123$	
morphology	Sp, Maximum peak height, nm	$1438 \pm 521$	$356 \pm 120$	
(area roughness	Sv, Maximum valley depth, nm	$2268 \pm 193$	$377 \pm 157$	
parameters)	Ssk, skewness	$-0.73 \pm 0.28$	-0.32±0.35	
	Sku, kurtosis	$3.98 \pm 1.15$	$3.00 \pm 0.33$	
	Sdr, developed interfacial area ratio, %	$18.25 \pm 5.61$	$1.31 \pm 1.62$	
	Al, mg kg <sup>-1</sup>	$2.46 \pm 0.03$	$1.22 \pm 0.24$	
Chemical	Fe, mg kg <sup>-1</sup>	$0.24 \pm 0.02$	$0.58 \pm 0.10$	
analysis	Ca, mg kg <sup>-1</sup>	$2.17 \pm 0.01$	$4.16 \pm 0.09$	
	Mg, mg kg <sup>-1</sup>	$0.25 \pm 0.02$	$0.60\pm0.01$	
BET surface area, m <sup>2</sup> /g		$0.029 \pm 0.007$	$0.012 \pm 0.001$	

QW and GF denote rough and relatively smooth sand, respectively.

Table S3. Calculated interaction energy parameters for AgNP-Sand interaction when pH=4 and 10 and the IS=5 mM: different surface roughness conditions

pН	$f_{sr}$	$f_{cr}$	$h_{sr}$	$h_{cr}$	$\Phi_{max}$ [-]	$\Phi_{1min}$ [-]
4	0	0	37	10	3.3	-58.6
10	0	0	37	10	53.1	28.2
4	0.05	0.5	37	10	0.0	-0.5
10	0.05	0.5	37	10	0.9	0.7
4	0.1	0.5	37	10	0.1	-1.1
10	0.1	0.5	37	10	1.8	1.4
4	0.2	0.5	37	10	0.2	-2.1
10	0.2	0.5	37	10	3.5	2.8
4	0.4	0.5	37	10	0.4	-4.2
10	0.4	0.5	37	10	7.1	5.6
4	0.8	0.5	37	10	0.9	-8.4
10	0.8	0.5	37	10	14.1	11.1

 $f_{cr}$ , nanoscale roughness fraction for colloid (AgNP);  $h_{cr}$ , high of  $f_{cr}$ , nm;  $f_{sr}$ , nanoscale roughness fraction for sand;  $h_{sr}$ , high of  $f_{sr}$ , nm;  $\Phi_{max}$ , energy barrier height;  $\Phi_{lmin}$ , depth of the primary minimum.